New measurement of neutron capture resonances in ^{209}Bi

C. Domingo-Pardo,[1,*] U. Abbondanno,[2] G. Aerts,[3] H. Álvarez-Pol,[4] F. Alvarez-Velarde,[5] S. Andriamonje,[3] J. Andrzejewski,[6] P. Assimakopoulos,[7] L. Audouin,[8] G. Badurek,[9] P. Baumann,[10] F. Bečvář,[11] E. Berthoumieux,[3] F. Calviño,[12] D. Cano-Ott,[5] R. Capote,[13,14] A. Carrillo de Albornoz,[15] P. Cennini,[16] V. Chepel,[17] E. Chiaveri,[16] N. Colonna,[18] G. Cortes,[12] A. Couture,[19] J. Cox,[19] M. Dahlfors,[16] S. David,[20] I. Dillman,[8] R. Dolfini,[21] W. Dridi,[3] I. Duran,[4] C. Eleftheriadis,[22] M. Embid-Segura,[5] L. Ferrant,[20] A. Ferrari,[16] R. Ferreira-Marques,[17] L. Fitzpatrick,[16] H. Frais-Koelbl,[13] K. Fujii,[2] W. Furman,[23] R. Gallino,[24] I. Goncalves,[17] E. Gonzalez-Romero,[5] A. Goverdovski,[25] F. Gramegna,[26] E. Griesmayer,[13] C. Guerrero,[5] F. Gunsing,[3] B. Haas,[27] R. Haight,[28] M. Heil,[8] A. Herrera-Martinez,[16] M. Igashira,[29] S. Isaev,[20] E. Jericha,[9] Y. Kadi,[16] F. Käppeler,[8] D. Karamanis,[7] D. Karadimos,[7] M. Kerveno,[10] V. Ketlerov,[16,25] P. Koehler,[30] V. Konovalov,[16,23] E. Kossionides,[31] M. Krtička,[11] C. Lamboudis,[7] H. Leeb,[9] A. Lindote,[17] I. Lopes,[17] M. Lozano,[14] S. Lukic,[10] J. Marganiec,[6] L. Marques,[15] S. Marrone,[18] P. Mastinu,[26] A. Mengoni,[13,16] P. M. Milazzo,[2] C. Moreau,[2] M. Mosconi,[8] F. Neves,[17] H. Oberhummer,[9] M. Oshima,[32] S. O'Brien,[19] J. Pancin,[3] C. Papachristodoulou,[7] C. Papadopoulos,[33] C. Paradela,[4] N. Patronis,[7] A. Pavlik,[34] P. Pavlopoulos,[35] L. Perrot,[3] R. Plag,[8] A. Plompen,[36] A. Plukis,[3] A. Poch,[12] C. Pretel,[12] J. Quesada,[14] T. Rauscher,[37] R. Reifarth,[28] M. Rosetti,[38] C. Rubbia,[21] G. Rudolf,[10] P. Rullhusen,[36] J. Salgado,[15] L. Sarchiapone,[16] I. Savvidis,[22] C. Stephan,[20] G. Tagliente,[18] J. L. Tain,[1] L. Tassan-Got,[20] L. Tavora,[15] R. Terlizzi,[18] G. Vannini,[39] P. Vaz,[15] A. Ventura,[38] D. Villamarin,[5] M. C. Vincente,[5] V. Vlachoudis,[16] R. Vlastou,[33] F. Voss,[8] S. Walter,[8] H. Wendler,[16] M. Wiescher,[19] and K. Wisshak[8]

(n_TOF Collaboration)

[1]*Instituto de Física Corpuscular, CSIC-Universidad de Valencia, Spain*

[2]*Istituto Nazionale di Fisica Nucleare, Trieste, Italy*

[3]*CEA/Saclay-DSM, Gif-sur-Yvette, France*

[4]*Universidade de Santiago de Compostela, Spain*

[5]*Centro de Investigaciones Energeticas Medioambientales y Technologicas, Madrid, Spain*

[6]*University of Lodz, Lodz, Poland*

[7]*University of Ioannina, Greece*

[8]*Forschungszentrum Karlsruhe GmbH (FZK), Institut für Kernphysik, Germany*

[9]*Atominstitut der Österreichischen Universitäten,Technische Universität Wien, Austria*

[10]*Centre National de la Recherche Scientifique/IN2P3-IReS, Strasbourg, France*

[11]*Charles University, Prague, Czech Republic*

[12]*Universitat Politecnica de Catalunya, Barcelona, Spain*

[13]*International Atomic Energy Agency, NAPC-Nuclear Data Section, Vienna, Austria*

[14]*Universidad de Sevilla, Spain*

[15]*Instituto Tecnológico e Nuclear(ITN), Lisbon, Portugal*

[16]*CERN, Geneva, Switzerland*

[17]*LIP-Coimbra & Departamento de Fisica da Universidade de Coimbra, Portugal*

[18]*Istituto Nazionale di Fisica Nucleare, Bari, Italy*

[19]*University of Notre Dame, Notre Dame, USA*

[20]*Centre National de la Recherche Scientifique/IN2P3-IPN, Orsay, France*

[21]*Università degli Studi Pavia, Pavia, Italy*

[22]*Aristotle University of Thessaloniki, Greece*

[23]*Joint Institute for Nuclear Research, Frank Laboratory of Neutron Physics, Dubna, Russia*

[24]*Dipartimento di Fisica, Università di Torino and Sezione INFN di Torino, Italy*

[25]*Institute of Physics and Power Engineering, Kaluga region, Obninsk, Russia*

[26]*Istituto Nazionale di Fisica Nucleare(INFN), Laboratori Nazionali di Legnaro, Italy*

[27]*Centre National de la Recherche Scientifique/IN2P3-CENBG, Bordeaux, France*

[28]*Los Alamos National Laboratory, New Mexico, USA*

[29]*Tokyo Institute of Technology, Tokyo, Japan*

[30]*Oak Ridge National Laboratory, Physics Division, Oak Ridge, USA*

[31]*NCSR, Athens, Greece*

[32]*Japan Atomic Energy Research Institute, Tokai-mura, Japan*

[33]*National Technical University of Athens, Greece*

[34]*Institut für Isotopenforschung und Kernphysik, Universität Wien, Austria*

[35]*Pôle Universitaire Léonard de Vinci, Paris La Défense, France*

[36]*CEC-JRC-IRMM, Geel, Belgium*

[37]*Department of Physics and Astronomy-University of Basel, Basel, Switzerland*

[38]*ENEA, Bologna, Italy*
[39]*Dipartimento di Fisica, Università di Bologna, and Sezione INFN di Bologna, Italy*
(Received 1 December 2005; published 23 August 2006)

The neutron capture cross section of ^{209}Bi has been measured at the CERN n_TOF facility by employing the pulse-height-weighting technique. Improvements over previous measurements are mainly because of an optimized detection system, which led to a practically negligible neutron sensitivity. Additional experimental sources of systematic error, such as the electronic threshold in the detectors, summing of γ-rays, internal electron conversion, and the isomeric state in bismuth, have been taken into account. γ-Ray absorption effects inside the sample have been corrected by employing a nonpolynomial weighting function. Because ^{209}Bi is the last stable isotope in the reaction path of the stellar *s*-process, the Maxwellian averaged capture cross section is important for the recycling of the reaction flow by α decays. In the relevant stellar range of thermal energies between $kT = 5$ and 8 keV our new capture rate is about 16% higher than the presently accepted value used for nucleosynthesis calculations. At this low temperature an important part of the heavy Pb-Bi isotopes are supposed to be synthesized by the *s*-process in the He shells of low mass, thermally pulsing asymptotic giant branch stars. With the improved set of cross sections we obtain an *s*-process fraction of 19±3% of the solar bismuth abundance, resulting in an *r*-process residual of 81±3%. The present (n, γ) cross-section measurement is also of relevance for the design of accelerator driven systems based on a liquid metal Pb/Bi spallation target.

DOI: 10.1103/PhysRevC.74.025807 PACS number(s): 25.40.Lw, 25.40.Sc, 27.80.+w, 97.10.Cv

I. INTRODUCTION

^{209}Bi is the end-point isotope of the *s*-process path. Its observed abundance has been finally understood in terms of the main *s*-process component, operating in the He-shell of low mass, low metallicity, thermally pulsing asymptotic giant branch (AGB) stars [1,2].

However, the complex production pattern at the end of the *s*-process path still hides important information, that can be unraveled by means of accurate neutron capture measurements. Capture on bismuth leads to the ground state of ^{210}Bi, which β decays to ^{210}Po that is α-unstable, producing ^{206}Pb (see Fig. 1).

However, given the ^{210}Po half-life of 138 days it can also act as a branching point by capturing another neutron and enhancing the abundance of ^{207}Pb instead. Another contribution to ^{207}Pb may be because of a long-lived isomer in ^{210}Bi at 271 keV. Neutron capture on this isomer leads to ^{211}Bi with an α-decay half-life of 2.17 min. The two branchings, at ^{210}Po and ^{210}Bi, depend strongly on the stellar conditions of neutron density and temperature. Given an appropriate stellar model and accurate neutron capture cross sections, the *s* abundances of the Pb/Bi isotopes can be more reliably determined, thus providing a better decomposition of the respective *r*-process abundances and of the radiogenic contributions because of the Th/U α decays. The latter information represents a viable constraint on the Th/U abundances calculation and its use as cosmochronometers [3,4].

For the discussion of these astrophysical aspects, the present status of the ^{209}Bi capture data is rather unsatisfactory [5]. Previous experiments exhibit significant discrepancies suggesting the existence of systematic uncertainties, which must be clearly reduced for a more quantitative assessment of the Pb/Bi abundances. Two capture resonance studies on ^{209}Bi have been reported so far, one at ORNL [6] and the other at GELINA [7,8]. In the former measurement, two strong *s*-wave resonances at low neutron energy could not be measured because of a low-neutron-energy cutoff at 2.6 keV. In addition, substantial corrections were needed for some of the resonances in order to account for the neutron sensitivity of the experimental setup employed. The GELINA measurement was also affected by significant corrections for neutron sensitivity.

The ^{209}Bi (n, γ) cross section has also a very practical application. Thanks to its properties of chemical inertness, high boiling point, low neutron moderation, and large scattering cross section, an eutectic mixture of lead and bismuth is presently considered as a very appropriate material for the spallation target and as the coolant for accelerator driven systems (ADS).

In a first sensitivity study of the neutron cross sections of the main materials used in this type of hybrid reactor [9], severe discrepancies were found between different evaluated nuclear data files. As a consequence, a list of isotopes was tagged for high priority measurements. Initially, most of the requested cross sections corresponded to the fuel and cladding materials and were focused on the elastic, inelastic, and (n, xn) channels. However, a recent extension of the same study [10] includes additional requests for the capture reactions in the spallation/coolant materials lead and bismuth. Comparing two evaluated data files, ENDF/B-VI.8 and JENDL 3.3, discrepancies in the neutron balance of 12.5% were identified to result from the uncertainties of the (n, γ) cross section of ^{209}Bi alone. Hence, the precise knowledge of the neutron capture cross sections of the lead and bismuth isotopes turned out to be of key relevance for the design of an ADS suited for the transmutation of radioactive residues and for energy production.

Apart from its contribution to the neutron balance, neutron capture on ^{209}Bi affects the radiotoxicity as well. Buildup of the α-emitters ^{210}Bi^m ($t_{1/2} = 3\times10^6$ yr) and ^{210}Po ($t_{1/2} =$

*Electronic address: Cesar.Domingo.Pardo@cern.ch

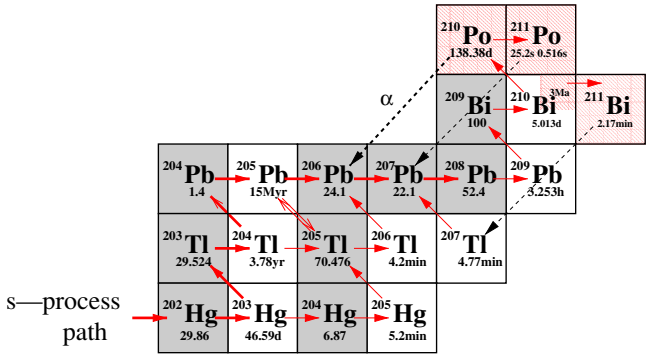

FIG. 1. (Color online) The *s*-process reaction network terminates at ^{209}Bi. Shaded boxes designate stable isotopes. Decays from the α-unstable ^{210,211}Po isotopes are represented with dashed lines. Quantities below the isotopic symbols show natural abundances or half-lives.

138 d) contributes to the long- and short-term radiotoxicity of the spallation target and of the coolant. These hazards can only be evaluated on the basis of a precise (n, γ) cross section of bismuth and with accurate data concerning the partial cross sections leading to ^{210}Bi^{m} and ^{210}Po.

II. CROSS-SECTION MEASUREMENT

The neutron energy differential capture cross section of ^{209}Bi has been measured at the n_TOF installation of CERN using the time-of-flight (TOF) technique. Because this facility has been described in detail elsewhere [11], only the main features are summarized in Sec. II A. The major motivation for this measurement was to overcome the systematic uncertainty related to the neutron-scattering background, which arises in measurements on isotopes with a dominant scattering channel. Sample scattered neutrons are easily captured in the materials surrounding the detector or in the sensitive detector volume itself, producing γ-rays, which appear as a prompt, TOF-dependent background. This effect becomes particularly crucial for the broad *s*-wave resonances in bismuth at low-neutron energies between 0.8 and 12 keV, resulting in corrections as large as 50% in previous measurements [6].

For this reason the reaction yield of this isotope has been measured with a set of total energy detectors consisting of optimized C_6D_6 liquid scintillation detectors (Sec. II B). This setup turned out to be of pivotal importance for the efficient suppression of the background from scattered neutrons. Other sample-related corrections were significantly reduced by choosing a comparably small bismuth sample 20 mm in diameter and 6.1 mm in thickness. The cross section is determined relative to the 4.9 eV ^{198}Au resonance by employing the saturated resonance technique [12]. For this purpose a gold sample 1 mm in thickness and 20 mm in diameter was measured in regular intervals. A thorough analysis of the capture data, including extensive Monte Carlo simulations of the necessary corrections to the experimental data, allowed us to determine the final cross section with a systematic uncertainty of better than 3%.

A. The n_TOF installation

At n_TOF, neutrons are produced via spallation reactions induced by 20 GeV protons in a lead target. Pulses of $(3–7)\times10^{12}$ protons with a duration of 6 ns (rms) hit the Pb-block with a typical repetition rate of 0.4 Hz. This very low duty cycle combined with the very high intensity in the beam pulses makes n_TOF an ideal facility for TOF measurements on radioactive samples. The low repetition rate has allowed to implement an advanced data acquisition system with zero dead time based on Flash-amplitude-to-digital converters [13].

The number of neutrons arriving at the sample are monitored by means of a 200-μg/cm^2-thick ^{6}Li foil centered in the beam. The particles emitted in the ^{6}Li$(n, \alpha)^3$H reaction are registered with four silicon detectors surrounding the ^{6}Li foil outside of the beam. The neutron monitor [14] is mounted in an evacuated carbon fiber chamber 3 m upstream of the samples. The samples, which are positioned at a flight path of 185 m, are fixed on a sample changer, which is also made of carbon fiber.

The neutron intensity has been determined by means of two independent measurements, performed with the Si-monitor described above and with a calibrated fission chamber [15]. Two measurements were carried out with the latter detector, employing foils of ^{235}U and ^{238}U. Calibration of the absolute yield in (n, γ) measurements via the saturated resonance method requires actually only the shape of the neutron flux, which can be directly determined from the Si-monitor and fission chamber measurements with an uncertainty below $\pm2\%$ [16].

The beam profile at the sample position has been determined to exhibit an approximate Gaussian shape with $\sigma =$ 7 mm, slightly off centered ($\Delta_x = 1.5$ mm) [17]. The samples used in this measurement cover about 60% of the neutron beam.

The excellent neutron energy resolution of the n_TOF facility is because of the long flight path of 185 m and the short proton pulse width. The resolution function was determined by means of Monte Carlo simulations [18] and has been validated experimentally by measuring narrow *p*- and *d*-wave capture resonances on a sample of $^{\text{nat}}$Fe.

B. Experimental setup

A general view of the experimental setup is shown in Fig. 2. The detection system used with the pulse-height-weighting technique (PHWT) [19] had been optimized with respect to the sensitivity for scattered neutrons, the most crucial source of background in (n, γ) studies on neutron magic nuclei, which are characterized by particularly large scattering-to-capture ratios. Scattered neutrons may be subsequently captured in the detectors or in nearby materials, where they produce γ-rays, which are likely to be registered with high probability, thus mimicking true capture events in the sample.

In an effort to reduce the neutron sensitivity as much as possible, special C_6D_6 liquid scintillation detectors [20] have been developed consisting of materials with low-neutron-capture cross sections. The main features of these detectors are thin-walled scintillator cells made of carbon fiber, which are

directly glued onto the photomultiplier tubes, thus eliminating dead materials, e.g., the common quartz window of the scintillator cells. To avoid the additional material of a support, the detectors were hanging on thin cords fixed at the ceiling. Similarly, the sample changer was made of carbon fiber as was the frame of the sample-holder. The samples were mounted on thin Kapton foils, which were glued on the frame that was much larger than the diameter of the neutron beam. In this way, the neutron sensitivity in the critical energy range from 1 to 100 keV could be reduced by factors of 3–10 [20].

The two detectors were placed at an angle of $\sim 125^\circ$ with respect to the sample to minimize the angular distribution effects of the primary capture γ rays. Also the background resulting from in-beam γ-rays scattered in the sample was considerably reduced in this configuration [21].

III. DATA ANALYSIS

In this section, the PHWT principle is reviewed together with the related systematic uncertainties of relevance for this type of capture measurements, followed by the determination of the weighting factors. We describe the calculation of accurate yield corrections and the analysis procedure to determine resonance parameters.

A. Pulse-height-weighting technique and systematic uncertainties

The PHWT is based on two conditions: (i) that the detector efficiency $\varepsilon_\gamma \ll 1$ so that at most only one γ ray per capture cascade is registered and (ii) that ε_γ is proportional to the energy of the registered γ-ray, $\varepsilon_\gamma \approx \alpha E_\gamma$. Under these two conditions, the efficiency ε_c for detecting a capture event, i.e., a cascade composed of m γ rays, becomes proportional to the sum energy E_c of that cascade. In this case one obtains

$$\varepsilon_c = 1 - \prod_{j=1}^{m}(1-\varepsilon_{\gamma j}) \approx \sum_{j=1}^{m}\varepsilon_{\gamma j} \approx \alpha E_c, \qquad (1)$$

which is a constant independent of the actual deexcitation pattern of the nucleus produced in the capture reaction. It is worth noting that the approximations in Eq. (1) are the better justified the better conditions (i) and (ii) are fulfilled.

The validity of Eq. (1) can be challenged by several experimental problems. In particular, condition (i) is violated if more than one γ ray of the cascade is registered in the same detector. Moreover, the product as well as the sum over the m γ rays of the cascade is always incomplete because of the unavoidable loss of γ rays because of electronic threshold applied to the detector signals, converted transitions, and partial population of the isomeric state in ^{210}Bi at 271 keV.

For all these effects, which may influence the validity of Eq. (1), appropriate corrections have to be determined as is shown in the following subsections.

As far as condition (ii) is concerned, the proportional increase of the efficiency with γ-ray energy is enforced by an appropriate modification of the detector energy response distribution $R(E)$. This is achieved by application of a pulse-height-dependent weighting factor W_i, such that the weighted sum of the response for a γ-ray j, R_{ij}, becomes proportional to its energy $E_{\gamma j}$,

$$\sum_i W_i R_{ij} = \alpha E_{\gamma j}. \qquad (2)$$

The second approximation in Eq. (1) depends directly on the accuracy of the calculated weights W_i, which can be tested as discussed below.

B. Weighting factors

It has been shown [22,23] that realistic response functions R_{ij} for mono-energetic γ rays with energies $E_{\gamma j}$ can be determined by means of Monte Carlo simulations for any particular setup for (n,γ) measurements. A set of expressions of the form of Eq. (2) can then be used to derive the weighting factors W_i.

The detailed geometry and chemical composition of the experimental setup has been implemented in the Monte Carlo simulation using GEANT4 [24] (see Fig. 2). The composition of the carbon fiber, which is by far the dominant structural material, was determined by an RBS analysis [25], yielding C/O/N/Ca/Br = 2.0/0.2/0.16/0.012/0.016. Also, the capture γ rays were carefully traced, assuming a radial distribution for the emission probability inside the sample according to the neutron beam profile described in Sec. II A. The depth distribution was included as well because it changed significantly from a practically uniform to a surface peaked shape between weak and strong resonances, respectively.

The weighting function (WF) of the gold calibration sample was obtained using the conventional approximation by a polynomial function of order $k = 4$, $W_i = \sum_{k=0}^{k=4} a_k E_i^k$. The values of the coefficients a_k were derived from a least-squares minimization,

$$\min \sum_j \left(\sum_i W_i R_{ij} - E_{\gamma j} \right)^2. \qquad (3)$$

Because of the higher γ-ray absorption in the 6.1-mm-thick bismuth sample the proportionality condition (ii) could

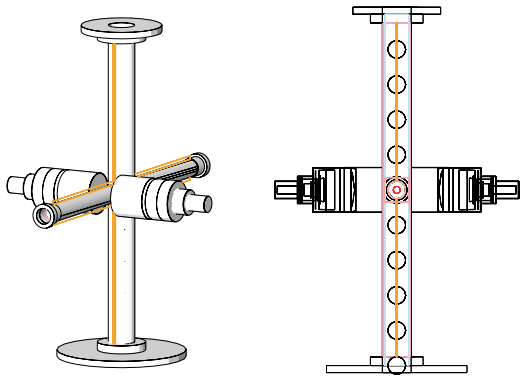

FIG. 2. (Color online) The geometry of the experimental setup used in the GEANT4 simulation of the weighting functions.

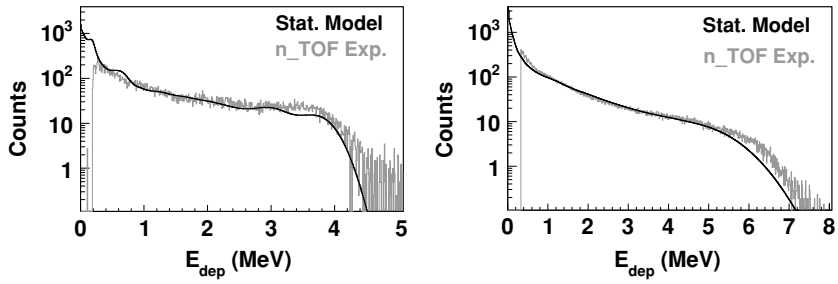

FIG. 3. Comparison of experimental (dashed) and simulated (solid) pulse height spectra of ^{210}Bi (left) and ^{198}Au (right) illustrating the quality of the simulations.

not be satisfied with the polynomial WF approach. In this case an accurate, pointwise WF was obtained by means of a linear regularization method for solving the inverse problem of Eq. (2) [16]. In this way the uncertainty connected with the polynomial WF has been reduced to 0.3%, an improvement by an order of magnitude.

The systematic uncertainty introduced by the WF was determined as described in Ref. [23], basically by performing Monte Carlo simulations of the capture cascades at a certain resonance. The deexcitation pattern is modeled by combining the experimentally known levels at low excitation energy with a statistical model of the nucleus to complete the cascade up to the capture energy. These simulated capture events can be used to estimate the uncertainty of the calculated WF.

To illustrate the performance of the cascade event generator for the samples measured in this experiment, the simulated pulse-height spectra R_i^C for the 802 eV resonance in ^{210}Bi and for the 4.9 eV resonance in ^{198}Au are compared in Fig. 3 with the corresponding experimental spectra measured at n_TOF.

The spectra based on the simulated cascades show in general a good agreement with the experimental spectra. The small differences at higher energy can be ascribed to the employed statistical model and to a lesser extent to the uncertainties in the calibration of the C_6D_6 detectors. In principle, these differences could be minimized by modifying the relative strength of $M1$ and $E1$ transitions in the statistical part of the cascades and/or the instrumental resolution. However, the effect on the weighted sum $\sum_i W_i R_i^C$ and, therefore, on the estimated uncertainty becomes absolutely negligible in both cases.

In summary, it was found that the simulated pulse height spectra can be employed for the determination of the uncertainty of the WF. By computing the weighted sum of each capture cascade with the calculated weighting functions, we obtain values, which deviate by less than 0.3% from the corresponding capture energies. This means that condition (ii) is fulfilled within 99.7%, leading to a practically negligible uncertainty because of the calculated WF.

C. Yield correction factors

The corrections for the electronic threshold, γ-summing, internal conversion, and the effect of the isomeric state (see Sec. III A) have been estimated by detailed Monte Carlo simulations of the capture events in a similar manner as in Ref. [23]. Although internal conversion and summing of cascade γ rays were found to have a minor effect of less than 2% on the capture yield of the bismuth sample, more significant corrections are required for the electronic threshold and for the isomeric state in ^{210}Bi. The isomeric state is included in the simulation by assigning a null branching ratio to the level of 271 keV, so that the deexcitation cascade ends at that level whenever it is reached.

The yield correction factor including all these effects can be calculated as

$$f^{t,s,\mathrm{ce},m} = \frac{n E_c}{\sum_{i=t} W_i R_i^C}, \tag{4}$$

where R_i^C is the total response of the detection system for n simulated capture events. For a threshold t of 200 keV, the yield correction factors calculated with this procedure for the bismuth sample are listed in the third column of Table I.

Because the simulated spectra for resonances with same spin and parity are very similar, i.e., almost independent of the resonance energy, the correction factors could be classified according to spin and parity of the resonance (first column in Table I).

The population of the isomeric state calculated with our statistical model of the nucleus is shown in the second column of Table I. For comparison, and to illustrate the possible uncertainty of the calculation, the correction factor of the hypothetic case, where the isomer is populated with 100% probability is shown in the last column. The differences were found to range between 1% and 2.5%.

As mentioned before, the cross section is determined relative to the 4.9-eV resonance in ^{197}Au. Therefore, the capture yield measured with the gold sample had to be corrected for experimental effects of threshold, γ-ray summing, and internal conversion. The corresponding correction factor for a threshold of 200 keV is $f_{\mathrm{Au}}^{t,s,\mathrm{ce}} = 1.046(2)$.

Hence, the final correction for each resonance is the ratio between the corresponding factor $f^{t,s,\mathrm{ce},m}$ from Table I and $f_{\mathrm{Au}}^{t,s,\mathrm{ce}}$. This ratio oscillates between 5% and 7%. It can be concluded, that the threshold, γ-summing, and internal

TABLE I. Yield correction factors for the bismuth sample calculated for a threshold of 200 keV.

J^π	Isom. popul.(%)	$f^{t,s,\mathrm{ce},m}$	$f^{t,s,\mathrm{ce},100\%m}$
3^+	6	1.124(2)	1.103(2)
4^-	8	1.131(2)	1.118(2)
4^+	9	1.143(2)	1.116(2)
5^-	23	1.137(2)	1.109(2)
5^+	22	1.142(2)	1.119(2)
6^+	44	1.134(2)	1.114(2)

conversion effects do not cancel out by measuring with respect to a reference sample. Neglecting these corrections could lead to systematic deviations in the yield determination of $\gtrsim$5%.

D. Neutron sensitivity

For a certain resonance at energy $E_\circ$ with capture and neutron widths, Γ_γ and Γ_n, the probability that a signal in the C_6D_6 scintillator is caused by a neutron scattered in the sample and eventually captured in the detector is given by

$$P^{\rm ns} = \left(\frac{\varepsilon_n}{\varepsilon_c}\right)\left(\frac{\Gamma_n}{\Gamma_\gamma}\right), \tag{5}$$

where ε_n denotes the probability of detecting a γ-ray produced by sample-scattered neutrons in or near the detector and ε_c the probability to register a γ-ray from a true capture cascade. This requires a correction of the experimental resonance yield by

$$f^{\rm ns} = \frac{1}{1+P^{\rm ns}}. \tag{6}$$

Equation (5) can be rewritten as,

$$P^{\rm ns} = \left(\frac{\varepsilon_n}{\varepsilon_\gamma}\right)\left(\frac{\varepsilon_\gamma}{\varepsilon_c}\right)\left(\frac{\Gamma_n}{\Gamma_\gamma}\right), \tag{7}$$

where ε_γ is the detection probability for a γ-ray of a given energy. For an energy $E_\gamma = 600$ keV, $\varepsilon_n/\varepsilon_\gamma$ has been calculated by means of Monte Carlo simulations for comparison with the experimentally determined value reported in Ref. [20]. The second factor, $\varepsilon_\gamma/\varepsilon_c$, has been determined by a detailed Monte Carlo simulation of the present experimental setup. The efficiency ε_γ was obtained for γ rays of 600 keV, whereas ε_c was determined using simulated capture cascades (see Secs. III B and III C). Finally, Γ_n/Γ_γ is to be determined by an iterative procedure of correcting and fitting the value of Γ_γ of the corresponding resonance.

In case of the s-wave resonance at 12.1 keV, which has the largest Γ_n/Γ_γ of all analyzed bismuth resonances, the corresponding ratios were found to be $\varepsilon_\gamma/\varepsilon_c = 0.446$ (this work) and $(\varepsilon_n/\varepsilon_\gamma)_{12.1\,\rm keV} = 1.5841\times10^{-5}$ [20]. Because of the very low neutron sensitivity the required correction for the 12.1-keV resonance of 3.6±0.7% is relatively small and practically negligible for the rest of the s-wave resonances in bismuth.

The 20% uncertainty of this correction results from neutron captures in the quartz window of the photomultiplier tube because of the uncertain silicon cross sections, which contribute a 10% uncertainty to $\varepsilon_n/\varepsilon_\gamma$, and from the resonance parameters Γ_n and Γ_γ, which exhibit uncertainties of 8% and 10%, respectively.

E. *R*-matrix analysis

The experimental yield

$$Y^{\rm exp} = f^{t,s,{\rm ce},m} f^{\rm ns} f^{\rm sat} \frac{N^w}{N_n E_c} \tag{8}$$

was determined by the weighted net count rate (N^w), the effective binding energy E_c, the integrated neutron flux N_n (obtained from the Si-monitor and from the shape of the neutron flux, Sec. II A), and the corrections discussed before. The factor $f^{\rm sat}$ corresponds to the absolute normalization via the analysis of the saturated resonance at 4.9 eV in ^{198}Au.

The yield has been analyzed with the multilevel R-matrix code SAMMY [26]. Using an iterative procedure based on Bayes's theorem, $Y^{\rm exp}$ is fitted with a function of the type,

$$Y^{\rm exp} = Y^f(E_\circ, \Gamma_n, \Gamma_\gamma) + B, \tag{9}$$

where Y^f corresponds to a parametrization as a function of the resonance parameters $E_\circ$, Γ_n, and Γ_γ according to the Reich-Moore formalism. For all partial waves a channel radius of 9.6792 fm was used. Whereas the well-known Γ_n values from transmission measurements were adopted, the resonance energies $E_\circ$ and capture widths Γ_γ have been fitted to the experimental data. The background below the resonance is described by the constant term B. In the fits with SAMMY, sample effects (single and double neutron scattering inside the sample) as well as thermal broadening are taken into account. The resolution function of the facility (Sec. II A) has been considered in the fits using the RPI parametrization.

The present results are illustrated in Fig. 4 at the example of the first two s-wave resonances in ^{210}Bi. The comparison with the capture yields calculated with the corresponding resonance parameters quoted in the ENDF/B-VI.8 evaluation demonstrates the improvement because of the reduced systematic uncertainties of the n_TOF data.

IV. RESULTS

In total, 21 resonances were identified in the ^{209}Bi(n,γ) data in the energy range from 800 to 23150 eV. The respective capture widths and areas are listed in Table II.

Beyond 23 keV further resonances could not be observed because of the in-beam γ-ray background [21], which was the major limitation in this experiment. However, this background

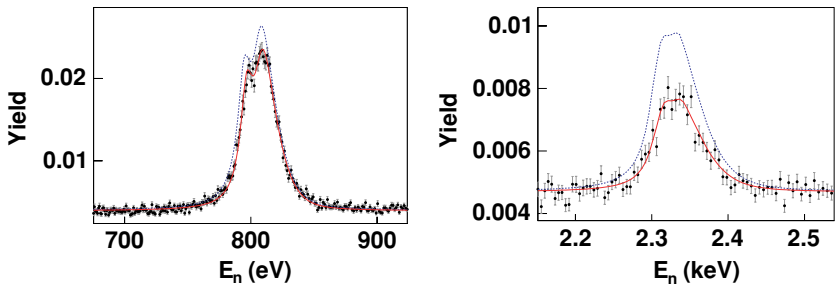

FIG. 4. (Color online) R-matrix analysis of the first two resonances in bismuth. The dashed line corresponds to the yield calculated with the resonance parameters quoted by the ENDF/B-VI.8 evaluation.

TABLE II. Resonance parameters[a] and radiative kernels[b] for ^{209}Bi.

$E_\circ$ (eV)	l	J	Γ_n (meV)	Γ_γ (meV)	$g\Gamma_\gamma\Gamma_n/\Gamma$ (meV)
801.6(1)	0	5	4309(145)	33.3(12)	18.2(6)
2323.8(6)	0	4	17888(333)	26.8(17)	12.0(8)
3350.83(4)	1	5	87(9)	18.2(3)	9.5(2)
4458.74(2)	1	5	173(13)	23.2(22)	11.3(11)
5114.0(3)	0	5	5640(270)	65(2)	35.3(11)
6288.59(2)	1	4	116(18)	17.0(17)	6.7(7)
6525.0(3)	1	3	957(100)	25.3(14)	8.6(5)
9016.8(4)	1	6	408(77)	21.1(14)	13.0(9)
9159.20(7)	1	5	259(45)	21.4(21)	10.9(11)
9718.910(1)	1	4	104(22)	74(7)	19.5(21)
9767.2(3)	1	3	900(114)	90(8)	28.7(26)
12098					65(4)[c]
15649.8(1.0)	1	5	1000	47(4)	20.2(17)
17440.0(1.3)	1	6	1538(300)	32(3)	20.4(18)
17839.5(9)	1	5	464(181)	43(4)	21.7(20)
20870	1	5	954(227)	34.4(33)	18.3(17)
21050	1	4	7444(778)	33(3)	14.8(13)
22286.0(9)	1	5	181(91)	33.6(32)	15.1(15)
23149.1(1.3)	1	6	208(154)	25.3(25)	14.7(15)

[a]Angular orbital momenta, l, resonance spins J, and neutron widths, Γ_n, are mainly from Refs. [27,28].

[b]Uncertainties are given as 18.2(6)≡18.2±0.6.

[c]This area corresponds to the sum of the areas of the broad s-wave resonance at the indicated energy, plus two p-wave resonances at 12.092 and 12.285 keV.

did not affect the initial aim of improving the systematic uncertainty of the broad s-wave resonances below 100 keV.

The capture areas determined at n_TOF are compared in Fig. 5 with the previous measurements performed at ORNL [6] and GELINA [7].

For most of the resonances shown in Fig. 5, there is a fair agreement with the ORNL data. However, significantly higher values are reported in the latter measurement for the two resonances at 3.3 and 5.1 keV and a lower cross section for the resonance at 9.77 keV. The GELINA data show agreement with n_TOF in several cases, but there is an average trend of lower cross sections. The largest differences in absolute values are for the resonances at 5.1 and 9.77 keV and the group at 12.1 keV. For these three resonances, the ORNL data show the opposite trend for the 5.1-keV resonance, agree with GELINA for the 9.77 keV resonance, and agree with the n_TOF data for the 12.1 keV group.

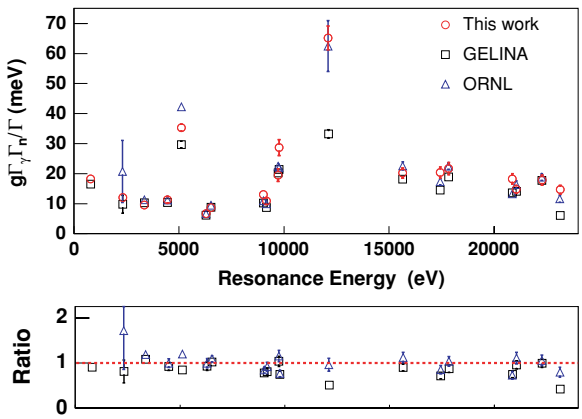

FIG. 5. (Color online) Comparison of the radiative capture kernels derived from the measurements at n_TOF, GELINA, and ORNL. The capture area shown at 2.3 keV for ORNL corresponds to an estimation reported in Ref. [6]. The capture area shown at ∼12 keV corresponds to the sum of the three resonances in that region.

The general systematics of better average agreement with the ORNL data and lower average values of the GELINA data, might be related to the weighting functions used in the respective experiments, although threshold correction effects (see Sec. III C) could play a role as well. Moreover, systematic deviations because of the neutron sensitivity corrections applied to some particular resonances cannot be excluded.

A. Discussion of uncertainties

The measuring technique employed in this work and the data-analysis procedures described in Secs. III and III C have been validated experimentally at n_TOF [23]. According to this study, the various contributions to the systematic uncertainty of the present data are about 2%. In addition, the energy dependence of the neutron flux has been found to exhibit an uncertainty of 2% as well, resulting in a total systematic uncertainty of better than 3%.

In this discussion, the neutron sensitivity correction has to be considered separately because it has been applied only to one of the measured resonances. Although the uncertainty of the correction was 20%, the contribution to the systematic uncertainty of the capture kernel was only 0.7% in this case.

V. IMPLICATIONS FOR THE *S*-ABUNDANCES IN THE PB-BI REGION

The slightly higher cross sections for *s*-wave resonances measured at n_TOF with respect to the values obtained at GELINA may affect the synthesis of the Pb/Bi. This holds preferentially at lower stellar temperature, because the neutron sensitivity correction becomes less relevant above 100 keV, where the relative contribution of the neutron-scattering channel decreases.

Qualitatively, the consequence of a higher ^{209}Bi cross section would reduce the survival probability and, hence, the *s*-process abundance of this isotope, but this could be compensated to some extent through an enhanced production through α-recycling via ^{206,207}Pb.

In the calculation of the Maxwellian averaged cross sections (MACS), the n_TOF resonances have been complemented between 25 and 31 keV with resonances from Ref. [7] and in the interval from 31 to 60 keV with capture areas from Ref. [27]. The additional resonances represent 2% and 7% of the MACS at $kT = 5$ and 8 keV, respectively. At lower stellar temperature, comparison of the results in Table III with the MACS obtained at GELINA [8] shows that the new values are 16% larger.

Beyond $kT = 20$ keV, the MACS is strongly influenced by the average capture cross section above 80 keV, which has been determined experimentally in Ref. [8]. For this reason, the differences obtained in the strong *s*-wave resonances at lower neutron energy do not affect substantially the MACS at 20–25 keV.

The MACS given in Table III refer to the lower temperature regime of the common stellar *s*-process site associated with thermally pulsing low mass AGB stars [29]. According to the Galactic chemical evolution (GCE) model described in Refs. [1,2], the *s*-process abundances of ^{208}Pb and ^{209}Bi are essentially produced in stars of low metallicity. In this model about 95% of the neutron exposure is because of the ^{13}C$(\alpha, n)^{16}$O reaction, which operates during the interpulse phase between He shell flashes at temperatures around $\sim 10^8$ K, corresponding to a thermal energy of $kT \approx 8$ keV.

The additional neutron irradiation provided by the ^{22}Ne$(\alpha, n)^{25}$Mg reaction at the higher thermal energy of $kT = 23$ keV during the He shell flash is rather weak. Hence, the abundances of isotopes with small cross sections are still dominated by what has been produced at the lower-temperature of the interpulse phase. Therefore, the low-temperature part of the MACS is important for this stellar model. With respect to the solar abundance tables of Anders and Grevesse [30], the GCE model [2] provides *s*-process abundances of ^{206}Pb, ^{207}Pb, and ^{209}Bi at the epoch of the solar system formation of 62%, 79%, and 19%, respectively.

According to the sensitivity study reported in Ref. [5], the present result (see Table III) is not expected to affect the abundances of ^{206,207}Pb by α-recycling from $A = 210$. This was confirmed by a model calculation for a thermally pulsing AGB star with $M = 3M_\odot$ and a metallicity [Fe/H] $= -1.3$, which yields a negligible difference for the abundances of ^{206}Pb and ^{207}Pb. The *s*-process abundance of ^{209}Bi itself was found to decrease only slightly from 19% to 18.7%.

To evaluate the uncertainty on the solar ^{209}Bi *s*-process fraction, we have to consider first the uncertainty in the cross section of this isotope in the two temperature regimes of the stellar model. The main contribution because of the uncertainty of the bismuth cross section is dominated by the conditions during the He shell flash. At the higher temperature of the ^{22}Ne$(\alpha, n)^{25}$Mg source ($kT = 23$ keV) the reaction flow via ^{208}Pb$(n, \gamma)^{209}$Bi is strongly enhanced over the situation during the ^{13}C$(\alpha, n)^{16}$O phase. This reflects the increase of the ^{208}Pb cross section with stellar temperature [31]. The net effect of the uncertainty on the ^{209}Bi cross section to its solar *s*-process abundance is found to be 6%.

In the evaluation of the final *s*-process abundance of bismuth, three aditional uncertainties have to be considered: (i) the effect of the uncertainty in the ^{208}Pb cross section, which directly affects the *s* production of ^{209}Bi by 6.5% (see Table VII in Ref. [5]), (ii) the 7%–8% uncertainty of the solar bismuth abundance (Refs. [30,32]), and (iii) a further 10% for the uncertainties related to the *s*-process model and for modeling GCE [2]. In summary the *s*-process contribution to solar bismuth is obtained as 19±3%, corresponding to an *r*-process residual of 81±3%.

This result is in agreement with the *r*-process calculation of Ref. [33] using the waiting point approximation and improved mass formulae, which yield an *r*-process contribution between 71% and 90%. A similar result is reported in Ref. [4], where the calculations give 77% and 92% *r*-process contributions depending on the initial seed composition.

TABLE III. Maxwellian averaged cross sections of ^{209}Bi compared to recent previous data.

kT (keV)	This work (mb)	Mutti *et al.* [8] (mb)
5	13.05(84)	11.25(58)
8	8.62(54)	7.48(44)
20	3.41(50)	3.34(42)
25	2.89(50)	2.85(45)

VI. ESTIMATION OF THE THERMAL CAPTURE CROSS SECTION

The thermal neutron capture cross section of ^{209}Bi can be expressed by the sum of the tails of all Breit-Wigner resonances,

$$\sigma_\gamma^{\mathrm{th}} \approx 4.099 \times 10^6 \left(\frac{A+1}{A}\right)^2 \sum_{i=1}^{N_\circ} g_n^i \frac{\Gamma_n^i \Gamma_\gamma^i}{(E_\circ^i)^2}. \qquad (10)$$

The result obtained with the resonance parameters from the present measurement (see Table II), is in agreement with that obtained from the GELINA measurement, as shown in Table IV. However, both values are around 40% smaller than the accepted value of 33.8(5) mb [27], which has been measured with the pile oscillator method. The direct

TABLE IV. Comparison of the thermal neutron capture cross section from different sources.

Cross section	Source	Ref.	$\sigma_\gamma^{\text{th}}$ (mb)
In-pile measurement		[27]	33.8(5)
From resonance parameters			
	This work		23.6(9)
	GELINA	[7]	24.6(9)
	ENDF		32.51
	JENDL		32.51

capture process cannot account for this discrepancy. In fact, a preliminary estimate of this component leads to a negligible contribution to the thermal cross-section value [34].

The resonance parameters of the ENDF and JENDL libraries have been adjusted to reproduce the in-pile $\sigma_\gamma^{\text{th}}$ measurement by means of an expression such as Eq. (10). With the improved, present data for the *s*-wave resonances this inconsistency could be removed by introducing subthreshold resonances in the evaluated data files.

VII. SUMMARY

At the CERN n_TOF facility the time-of-flight method has been employed with the pulse-height-weighting technique to determine the neutron-capture cross section of bismuth in the resolved resonance region.

The main improvement with respect to previous measurements is because of an optimized detection setup, by which the crucial neutron sensitivity could be considerably reduced. All remaining sources of systematic uncertainties have been thoroughly treated by detailed Monte Carlo simulations. Resonance energies ($E_\circ$), widths (Γ_γ), and capture areas have been determined by an *R*-matrix analysis covering the energy range from 0.8 to 23 keV. The results show larger capture areas for the *s*-wave resonances, yielding a 16% enhancement of the stellar neutron capture rate at thermal energies between 5 and 8 keV compared with recent data [8]. The new cross section results for ^{209}Bi, combined with recent improvements in the cross section of ^{208}Pb [5], yield a solar *s*-process abundance of 19(3)% for bismuth. The resulting *r*-process residual of 81(3)% represents a reliable constraint for *r*-process calculations [33].

ACKNOWLEDGMENTS

We acknowledge the help of G. Arbanas (ORNL) in providing the direct capture contribution to the thermal cross section. R.G. and F.K. appreciate the opportunity to discuss this article at the Aspen Summer School organized in 2005 by R. Reifarth and F. Herwig. This work was supported by the European Commission (FIKW-CT-2000-00107), by the Spanish Ministry of Science and Technology (FPA2001-0144-C05), and partly by the Italian MIUR-FIRB grant "The astrophysical origin of the heavy elements beyond Fe." It is part of the Ph.D. thesis of C.D., who acknowledges financial support from Consejo Superior de Investigaciones Científicas.

[1] C. Travaglio, D. Galli, R. Gallino, M. Busso, F. Ferrini, and O. Straniero, Astrophys. J. **521**, 691 (1999).
[2] C. Travaglio, R. Gallino, M. Busso, and R. Gratton, Astrophys. J. **549**, 346 (2001).
[3] J. J. Cowan, F.-K. Thielemann, and J. W. Truran, Phys. Rep. **208**, 267 (1991).
[4] K.-L. Kratz, B. Pfeiffer, J. J. Cowan, and C. Sneden, New Astron. Rev. **48**, 105 (2004).
[5] U. Ratzel, C. Arlandini, F. Käppeler, A. Couture, M. Wiescher, R. Reifarth, R. Gallino, A. Mengoni, and C. Travaglio, Phys. Rev. C **70**, 065803 (2004).
[6] R. Macklin and J. Halperin, Phys. Rev. C **14**, 1389 (1976).
[7] P. Mutti, Ph.D. Thesis, University of Gent, 1997.
[8] P. Mutti, F. Corvi, K. Athanassopulos, H. Beer, and P. Krupchitsky, in *Nuclei in the Cosmos*, edited by N. Prantzos and S. Harissopulos (Editions Frontières, Volos, 1998), pp. 204–207.
[9] C. Rubbia *et al.*, 1st Management Report of the n_TOFND-ADS EC programme under contract no. FIKW-CT-2000-00107.
[10] A. Herrera, M. Dahlfors, Y. Kadi, and G. T. Parks, in *Workshop on Nuclear Data for the Transmutation of Nuclear Waste*, edited by A. Kelic and K. Schmidt (Darmstadt, Germany, 2003).
[11] The n_TOF Collaboration, CERN n_TOF Facility: Performance Report, CERN/INTC-O-011 INTC-2002-037 CERN-SL-2002-053ECT, 2002 (unpublished).
[12] R. Macklin, J. Halperin, and R. Winters, Nucl. Instrum. Methods A **164**, 213 (1979).
[13] U. Abbondanno, G. Aerts, F. Alvarez, H. Alvarez, S. Andriamonje, J. Andrzejewski, G. Badurek, P. Baumann, F. Becvar, J. Benlliure *et al.*, Nucl. Instrum. Methods A **538**, 692 (2005).
[14] S. Marrone, P. F. Mastinu, U. Abbondanno, R. Baccomi, E. B. Marchi, N. Bustreo, N. Colonna, F. Gramegna, M. Loriggiola, S. Marigo *et al.*, Nucl. Instrum. Methods A **517**, 389 (2004).
[15] PTB group, n_TOF neutron fluence with the PTB Fission Chambers, CERN/SL/ECT/2002, 2002 (unpublished).
[16] C. Domingo-Pardo, Ph.D. Thesis, CSIC-University of Valencia, 2005.
[17] J. Pancin, U. Abbondanno, G. Aerts, H. Alvarez, S. Andriamonje, A. Angelopoulos, P. Assimakopoulos, C. Bacri, G. Badurek, P. Baumann *et al.*, Nucl. Instrum. Methods A **524**, 102 (2004).
[18] C. Coceva, M. Frisoni, M. Magnani, and A. Mengoni, Nucl. Instrum. Methods A **489**, 346 (2002).
[19] R. L. Macklin and J. H. Gibbons, Phys. Rev. **159**, 1007 (1967).
[20] R. Plag, M. Heil, F. Käppeler, P. Pavlopoulos, R. Reifarth, K. Wisshak, and (n_TOF Collaboration), Nucl. Instrum. Methods A **496**, 425 (2003).
[21] U. Abbondanno *et al.*, CERN Report No. CERN-SL-2002-053 ECT, 2003 (unpublished).

[22] J. L. Tain, F. Gunsing, D. Cano-Ott, N. Colonna, C. Domingo, E. Gonzalez, M. Heil, F. Käppeler, S. Marrone, P. Mastinu *et al*., J. Nucl. Sci. Technol. **2**, 689 (2002).
[23] U. Abbondanno, G. Aerts, H. Alvarez, S. Andriamonje, A. Angelopoulos, P. Assimakopoulos, C. O. Bacri, G. Badurek, P. Baumann, F. Bečvár *et al*., Nucl. Instrum. Methods A **521**, 454 (2004).
[24] Geant4 Collaboration, S. Agostinelli, J. Allison, K. Amako, J. Apostolakis, H. Araujo, P. Arce, M. Asai, D. Axen, S. Banerjee *et al*., Nucl. Instrum. Methods A **506**, 250 (2003).
[25] C. Domingo-Pardo, Diploma Thesis, CSIC-University of Valencia, 2001.
[26] N. Larson, SAMMY: Multilevel *R*-matrix fits to neutron data using Bayes equations, ORNL/TM-9179, 2000 (unpublished).
[27] S. F. Mughabghab, *Neutron Cross Sections: Neutron Resonance Parameters and Thermal Cross Sections* (Academic Press, New York, 1984).
[28] S. I. Sukhoruchkin, Z. N. Soroko, and V. V. Deriglazov, *Low Energy Neutron Physics: Tables of Neutron Resonance Parameters* (Springer, Landolt-Börnstein, 1998), Vol. I/16B.
[29] R. Gallino, C. Arlandini, M. Busso, M. Lugaro, C. Travaglio, O. Straniero, A. Chieffi, and M. Limongi, Astrophys. J. **497**, 388 (1998).
[30] N. Grevesse and E. Anders, Geovesse et Cosmochimica Acta. **53**, 197 (1989).
[31] H. Beer, F. Corvi, and P. Mutti, Astrophys. J. **474**, 843 (1997).
[32] K. Lodders, Astrophys. J. **591**, 1220 (2003).
[33] J. J. Cowan, B. Pfeiffer, K.-L. Kratz, F.-K. Thielemann, C. Sneden, S. Burles, D. Tytler, and T. C. Beers, Astrophys. J. **521**, 194 (1999).
[34] G. Arbanas (ORNL) (private communication).